UNIVERISTY OF OKLAHOMA

GRADUATE COLLEGE

QUANTIFYING PRECIPITATION EFFICIENCY AND DRIVERS OF EXCESSIVE PRECIPITATION IN POST-LANDFALL HURRICANE HARVEY

A THESIS

SUBMITTED TO THE GRADUATE FACULTY

in partial fulfillment of the requirements for the

Degree of

MASTER OF SCIENCE IN METEOROLOGY

By

Noah Brauer

Norman, Oklahoma

2019

QUANTIFYING PRECIPITATION EFFICIENCY AND DRIVERS OF EXCESSIVE PRECIPITATION IN POST-LANDFALL HURRICANE HARVEY

A THESIS APPROVED FOR THE

SCHOOL OF METEOROLOGY

BY

Dr. Jeffrey B. Basara, Chair

Dr. Cameron R. Homeyer

Dr. Greg M. McFarquhar

Acknowledgements

The authors thank Ryann Wakefield, Jordan Christian, Greg Jennrich, Addison Alford, and Jason Furtado for their constructive feedback, comments, and guidance towards this work. Additionally, the authors thank Travis Smith, Micheal Simpson, Heather Reeves, and Kiel Ortega at CIMMS and the NOAA National Severe Storms Laboratory for processing and providing the MRMS radar-derived rotation tracks that were used in this study.

Contents

Abstract

Hurricane Harvey produced widespread rainfall amounts over 1000 mm in portions of Southeast Texas, including Houston, from 26-31 August 2017. The highly efficient and prolonged warm rain processes associated with Harvey played a key component in the catastrophic flooding that occurred throughout the region. Precipitation efficiency (PE) is widely referred to in the scientific literature when discussing excessive precipitation events that lead to catastrophic flash flooding, but has yet to be explored or quantified in tropical cyclones coincident with polarimetric radar observations. With the introduction of dual-polarization radar to the NEXRAD WSR-88D network, observed polarimetric radar variables such as Z_H, Z_{DR}, and K_{DP} can be used to gain insight into the precipitation processes that contribute to enhanced PE. It is found that 6-hour mean values of Z_H between 35-45 dBZ, Z_{DR} between 1-1.5 dB, and K_{DP} greater than 1.5 degrees/km were collocated with the regions of PE greater than 100% between 27-29 August. Additionally, supercell thunderstorms embedded in the outer bands of Harvey were identified via 3-6 km MRMS rotation tracks and were found to be collocated with swaths of enhanced positive Z_H, Z_{DR}, and K_{DP}. The $R(K_{DP}, Z_{DR})$ relationship demonstrated that 1-hour mean rainfall rates in these supercells were as high as 85 mm/hour and played a significant contribution to the excessive precipitation event that occurred over the region.

1 Introduction

Excessive precipitation events that result in flooding are the second-deadliest meteorological hazard after excessive heat (Ashley and Ashley 2008). Although flooding tends to be particularly detrimental to life and property in developing countries, in recent years developed countries such as the United States have had impactful events when flooding is collocated with large population centers. The overall severity of the flooding depends not only on the rainfall rate and the duration of the heavy precipitation, but also land use of the region, topography, and antecedent moisture prior to the event.

Landfalling tropical cyclones that have formed in the Atlantic Basin are responsible for an estimated 0.5 million fatalities since 1492, including 25,000 deaths in the United States (e.g., Rappaport and Fernandez-Partagas 1997; Rappaport 2000; Rappaport 2014). While storm surge poses a major threat to coastal areas, excessive precipitation events associated with tropical cyclones can occur hundreds of miles inland have been responsible for thousands of fatalities in North America. For example, tropical storm Allison produced catastrophic flooding in Southeast Texas in 2001, with a total rainfall accumulation of 940 mm observed at the Port of Houston and a resulting 24 deaths (Service 2001).

Radar observations from the WSR-88D network are useful in cases of landfalling tropical cyclones as they provide observations at a high temporal resolution (e.g., Medlin et al. 2007; Didlake Jr. and Kumjian 2018) allowing for the identification of

mesoscale features contained within the spiral rainbands and eyewall. The processes occurring in these features can ultimately enhance rainfall rates at the surface. Traditionally, the equivalent radar reflectivity factor at a horizontal polarization (Z_H) has been used to estimate the surface rainfall rate using a Z-R relationship. Such relationships between Z_H and rainfall rate (R) are typically derived empirically (e.g., Rosenfeld et al. 1993; Crosson et al. 1996), and depend on the drop size distribution and other factors such as the presence of partial beam filling and path attenuation (e.g., Rosenfeld et al. 1993; Ryzhkov et al. 2005b). Thus, the use of Z-R relationships may be useful for determining the threat of flash flooding in warning operations, but may become problematic when the drop size distribution varies between the convective and the stratiform components of tropical cyclones, so a single relationship does not apply. Additionally, this method must be applied to the entire 360^o azimuth, and errors arise when microphysical processes vary throughout the radar domain (e.g., Zrnić and Ryzhkov 1996; Ryzhkov et al. 2005b; Kumjian 2013b).

Only recently, since 2010, has the addition of dual-polarization radar to the WSR-88D network (Istok et al. 2009) allowed for the evolution of precipitation processes in landfalling tropical cyclones in the Continental United States to be better understood. The incorporation of polarimetric radar observations in the WSR-88D network allows for additional insight regarding the evolution of the drop size distribution, microphysics, and number concentration of hydrometeors (e.g., Seliga and Bringi 1976; Herzegh and Jameson 1992; Zrnic and Ryzhkov 1999; Kumjian 2013a), which can

be used to provide more accurate and precise Z-R relationships in heavy precipitation events associated with tropical rainfall. Dual-polarization radar also allows for the utilization of differential reflectivity (Z_{DR}) and specific differential phase (K_{DP}) to estimate rainfall rates without the assumption of an empirical Z-R relation (e.g., Ryzhkov et al. 2005b; Giangrande and Ryzhkov 2008; Cifelli et al. 2011).

In tropical environments, Houze 1997 demonstrated that precipitation in stratiform rain events is primarily driven by warm rain processes whereas convective precipitation introduces additional cold rain processes when updrafts extend above the -10^oC level (Vitale and Ryan 2013). This results in the presence of supercooled liquid drops above the melting level (e.g., Vitale and Ryan 2013; Schroeder et al. 2016). For this reason, the warm cloud depth (WCD) is defined as the layer between the cloud base and the -10^o level, to account for the presence of supercooled liquid drops that can also contribute to collision-coalescence. From Houze 1997, stratiform regions in a tropical environment can be defined as precipitation occurring in regions with weaker, decaying convection, along with the presence of a bright band in the Z_H field, which generally occurs in areas of weak ascent. Convective regions are defined as areas of ascent greater than 1 ms^{-1} and developing young, or mature convection (Houze 1997).

The convective features in excessive precipitation events can be identified using polarimetric radar by recognizing columns of enhanced positive Z_{DR} extending above the 0^oC level. These indicate convective updrafts lofting supercooled drops above the

melting layer in continental convection (e.g., Herzegh and Jameson 1992; Loney et al. 2002; Kumjian et al. 2014). Lastly, van Lier-Walqui et al. 2016 show that columns of positive K_{DP} can be translated to water-coated ice or supercooled liquid being lofted above the 0^oC isotherm as well, and can be used as a proxy for convective updrafts.

A critical component of hydrometerology that has not yet been explored is the relationship between polarimetric radar observations and precipitation efficiency (PE). Ye et al. 2014 define PE as the quotient of total precipitable water (TPW) to the total precipitation accumulation at the surface at the same location within a temporal period, and can be used to determine the amount of available tropospheric water vapor that can be removed from a vertical column at a given time and location (e.g., Doswell et al. 1996; Anip 2005; Hisham Mohd Anip and Market 2007; Ye et al. 2014). While TPW varied from 26-29 August by 20 mm, TPW from 26-28 August only varied by 12 mm and was relatively constant throughout a local domain on a daily timescale, but precipitation is highly variable spatially and temporally (Doswell et al. 1996). As a result, PE near or greater than 100% can be translated to mesoscale and storm-scale dynamic processes with large, strong updrafts (Doswell et al. 1996) that ultimately lead to condensation and heavy precipitation.

Typically excessive precipitation events that result in flooding occur where the rainfall rate is heaviest for the longest period of time (e.g., Chappell 1986; Doswell et al. 1996). While previous studies have examined precipitation processes and hydrometeorological impacts of landfalling tropical cyclones using airborne observations,

reanalysis fields, and satellite data, post-landfall Hurricane Harvey in 2017 provides an opportunity to specifically examine hydrometeorological drivers of excessive precipitation and flooding using polarimetric radar observations. As such, this study aims to quantify PE in both the convective and stratiform elements that contributed to the flooding in Houston using polarimetric radar observations from the KHGX WSR-88D, observed radiosonde data, Multi-Radar Multi-Senor (MRMS) radar-derived rotation tracks, and North American Regional Reanalysis (NARR). The supercells that were identified in the outer rainbands of Harvey were found to have positive enhancements of the polarimetric radar variables, translating to an increase in rainfall rate and PE.

In addition, supercell thunderstorms are known to locally enhance rainfall rates due to their strong updrafts in the presence of rotation (Nielsen and Schumacher 2018). Traditional supercells that develop in continental air and are influenced by baroclinic instability are known to have a PE$<$ 100% due to the influence of hail, deep-layer shear resulting in limited drop residence time, and additional cold rain processes (eg., Marwitz 1972; Foote and Fankhauser 1973; Browning 1977). Despite continental supercells having low PE, they are capable of producing extreme rainfall rates which can ultimately lead to flash flooding and loss of life and property (e.g., Smith et al. 2001; Duda and Gallus 2010; Hitchens and Brooks 2012). Further, supercells are able to maintain their updrafts for a longer duration compared to non-rotating storms because of the associated non-linear hydrodynamic vertical perturbation pressure gradient force (e.g., Weisman and Klemp 1984; Doswell et al. 1996). In addition,

Doswell et al. 1996 found that the intense, rotating updrafts found in supercells increase the probability for heavy rainfall rates, which would otherwise be less likely if rotation did not exist.

Numerous supercells were observed in the outer rainbands of Harvey which produced 52 tornadoes, particularly in and to the south of Houston (National Hurricane Center). Overall, the PE of supercells within a tropical cyclone environment such as Harvey have yet to be explored. This study hypothesizes that prolonged training of supercells within the outer rainbands of Harvey over Houston have a significantly higher PE due to an environment characterized by anomalous precipitable water in addition to considerable moisture flux convergence and latent heat fluxes translating to an increase in available tropospheric moisture from condensation. Further, given Harvey's long duration and an environment characterized by anomalously high TPW and deep WCD, the combination of these elements resulted in the extended flooding event over Southeast Texas with locally excessive rainfall totals as high as 1500 mm. As such, a second goal of this study is to examine the rotating features within the outer rainbands of Harvey, and their relationship to PE and enhanced rainfall rates using the available datasets in combination with Multi-Radar-Multi-Sensor (MRMS) radar-derived rotation tracks.

2 Data and Methods

2.1 Event Background

From 26 Aug 2017 to 30 Aug 2017, Hurricane Harvey produced over 1500 mm (60 in) of rain in localized areas within the Houston Metropolitan Area with widespread precipitation accumulations of 1000 mm throughout southeast Texas (National Weather Service Houston/Galveston 2017; Figure 1). Harvey made landfall near Rockport, Texas at 0300 UTC 26 August as a Category 4 hurricane with maximum sustained winds of 115 knots and a minimum central pressure of 937 hPa, and produced widespread wind damage and storm surge. As Harvey progressed north, it weakened to a tropical storm by 1800 UTC 26 August before reversing track to the southeast, eventually moving back over the Gulf of Mexico at 1200 UTC 28 August. At this time, the outer rainbands from Harvey produced training convective and stratiform precipitation over Houston which led to catastrophic flooding and multiple all-time rainfall records being broken; Tropical Storm Amelia had previously held the record for the highest rainfall amount from a tropical cyclone in the continental United States, with 1219 mm in 1979 (National Hurricane Center). In contrast, during post-landfall Harvey, 18 stations across southeast Texas reported rainfall amounts over 1219 mm during Harvey. Harvey made its final landfall over extreme southwestern Lousiana on 0800 UTC 30 August as a tropical storm before moving northeast and making a complete extratropical transition by 0600 UTC 1 September over the

Tennessee Valley (Fig. 2).

2.2 Reanalysis Data

The North American Regional Reanalysis (NARR) dataset which uses a 32-km resolution grid projected onto a Northern Hemisphere Lambert Conformal Conic Grid (Mesinger et al. 2006) was used to calculate and plot PE over southeast Texas. Reanalysis fields of total accumulated precipitation and total precipitable water (TPW) were used from 25-30 August 2017 to calculate PE, which can be expressed mathematically as (1). Daily PE values from 26-30 August at the Corpus Christi, TX (CRP; 27.98686^{o}N, $-$97.23364^{o}W) and Lake Charles, LA (LCH; 30.45164^{o}N, $-$92.94987^{o}W) upper air stations are also displayed in Table 2.

$$PE = \frac{Total\ Precipitation\ Accumulation}{TPW} \tag{1}$$

Latent heat flux anomalies were computed using the 1979-2017 climatology by removing the weekly mean from each day. These data were then standardized using the weekly standard deviation and the daily mean 10-m wind vectors were overlayed to provide a qualitative sense of moisture advection for each day. Additionally, TPW anomalies during the same period were standardized using the daily 1979-2017 mean

and standard deviation.

The Parameter-elevation Regressions on Independent Slopes Model (PRISM) was used for daily precipitation accumulation from 26-30 August over Southeast Texas, and has a 4 km grid resolution. More information regarding the data processing and projections can be found in Daly et al. 1994

2.3 Polarimetric Radar Observations

The long duration of Harvey adjacent to the coast provided a unique opportunity to explore polarimetric radar signatures associated with a landfalling tropical cyclone given multiple NEXRAD WSR-88D radars obtained dual-polarization observations during landfall and the subsequent heavy rainfall event. The polarimetric radar data have a temporal resolution of $\sim$ 5 minutes, a spatial resolution of 1 km, and uses a polar grid (Crum and Alberty 1993). Additionally, each radar has an azimuthal resolution of 0.5 degrees below 7.0 km and 1.0 degree resolution up to 22.0 km. The variables analyzed in this study include the Z_H, Z_{DR}, and K_{DP}. The Level-II WSR-88D data used in this study is from the National Centers for Environmental Information (Center 1991; Crum and Alberty 1993), and were then processed using GridRad software (Bowman and Homeyer 2017), which includes numerous quality control and filtering techniques, and has a spatial resolution of 0.2^o x 0.2^o.

The equivalent radar reflectivity factor at a horizontal polarization (Z_H) is proportional to the integration of the diameter of scatterers within a radar volume raised

to the sixth power (e.g., Austin 1987; Herzegh and Jameson 1992; Zrnic and Ryzhkov 1999; Kumjian 2013a; Vitale and Ryan 2013) and provides information regarding the size and concentration of Rayleigh scatterers (e.g., Austin 1987; Herzegh and Jameson 1992; Zrnic and Ryzhkov 1999; Kumjian 2013a). The Z_{DR} is defined as the difference in the horizontal and vertical reflectivity factors, and is dependent on the size, shape, and orientation of hydrometeors (e.g., Seliga and Bringi 1976; Herzegh and Jameson 1992). One must be cautious when using Z_{DR} since these measurements can be biased in the presence of mixed-phase precipitation, leading to non-uniform beam-filling, as well as differential attenuation (e.g., Bringi et al. 1990; Testud et al. 2000; Ryzhkov 2007; Giangrande and Ryzhkov 2008; Kumjian 2013b; Kumjian 2013c). The K_{DP} field is useful for determining the number concentration of raindrops in a radar volume (Kumjian 2013b). Because large raindrops are oblate, there will be more of a phase lag in the horizontal polarization relative to the vertical polarization as more drops are encountered in the horizontal, yielding positive K_{DP} (e.g., Seliga and Bringi 1976; Herzegh and Jameson 1992; Zrnić and Ryzhkov 1996; Ryzhkov et al. 2005a; Ryzhkov et al. 2005b; Kumjian 2013a). Lastly, the co-polar correlation coefficient between the horizontal and vertical polarizations (ρ_{hv}) can be used to quantify the diversity of scatterers in a sample volume (e.g., Herzegh and Jameson 1992; Ryzhkov et al. 2005a; Ryzhkov et al. 2005b; Kumjian 2013a). More uniform scatterers such as rain will result in a ρ_{hv} close to 1, whereas mixed-phase precipitation will yield a $\rho_{hv} < 0.9$ (e.g., Herzegh and Jameson 1992; Zrnic and Ryzhkov 1999; Ryzhkov et al.

2005a; Ryzhkov et al. 2005b; Kumjian 2013a). As noted by Kumjian 2013a, Z_{DR} is independent of the number concentration of hydrometeors, but can be used in unison with K_{DP} to gain insight of the characteristics and intensity of ongoing precipitation. In the case of tropical cyclones, K_{DP} values near 1 deg/km and Z_{DR} values between 0-1 dB implies a large number concentration of small drops (e.g., Brown et al. 2016; Didlake and Kumjian 2017). For this reason, regions of highest PE are expected to be largely collocated with the regions of highest Z_H, Z_{DR}, and K_{DP}.

K_{DP} is computed via a centered difference method of the raw differential phase shift (ϕ_{DP}) observations and are then smoothed to minimize noise. Additionally, gridpoints where $\rho_{hv} < 0.5$ are neglected as these points are largely representative of non-meteorological scatterers. A detailed description and analysis of these algorithms can be found in Bowman and Homeyer 2017.

The 1-hour and 6-hour means of Z_H, Z_{DR}, and K_{DP} were computed at 2 and 3 km to minimize noise from melting precipitation and bright-banding that occurred within the 4-5 km layer and acts to positively-bias Z_H and Z_{DR}. This is because melting snowflakes gain a liquid coating on the outer portions of the crystals, which increases the overall reflectivity of the hydrometeors and therefore the Z_H (e.g., Herzegh and Jameson 1992; Ryzhkov et al. 2005a; Ryzhkov et al. 2005b;Kumjian 2013a). Additionally, the enhanced positive Z_{DR} caused by melting snow aggregates results in an greater horizontal polarization compared to the vertical, and thus a highly positive Z_{DR}. The 2 km and 3 km levels were also chosen to minimize noise from ground

clutter that is apparent in the lower 1.0 and 1.5 km scans.

Time-height curtains of Z_H, Z_{DR}, and K_{DP} are plotted from 26-30 August with a 5 data point radius around Houston, Texas with a latitude and longitude of 29.7396^{o}N and -95.3854^{o}W, and a 5 data point radius around Liberty, Texas with coordinates of 30.0554^{o}N and -94.7932^{o}W. A spatial mean was then computed over the 5 surrounding grid points and was used to plot the vertical profiles, similar to the quasi-vertical profile methodology in Ryzhkov et al. 2016. These points were subjectively chosen to gain insight to the vertical distribution polarimetric radar variables, and how they varied spatially between different portions of the outer rainbands of Harvey.

Raw NEXRAD-WSR 88D radar data from the KHGX (Houston) radar were used to plot a single-site radar image of 0.5^o Z_H and 1.5^o storm-relative velocity at 0331 UTC 27 August. Higher elevation tilts were used to better identify mesocyclones that were in close proximity to KHGX, whereas 1.5^o Z_H data were unavailable for the times of the images. Both Z_H and storm-relative velocity data has a spatial resolution of 1 km (Crum and Alberty 1993).

Finally, radar-derived rainfall rates and precipitation accumulations were derived using the $R(K_{DP}, Z_{DR})$ relationship determined by Zhang et al. 2018 and described in Equation 2. This quantitative precipitation estimation (QPE) algorithm was found to perform best when $Z_H \geq 38$ dBZ, $K_{DP} \geq 1$ deg/km, and $Z_{DR} \geq 1$ dB, using the constants $a = 51.16$, $b = 0.9311$, and $c = -0.0852$ which are empirically derived and are best used in convective, warm rain events (Zhang et al. 2018). 1-hour rainfall

rates were computed using the 1-hour means of Z_H, Z_{DR}, and K_{DP} at 2 km. 6-hour mean rainfall rates were also calculated by averaging the 1-hour mean rainfall rates over six hour periods.

$$R(K_{DP}, Z_{DR}) = aK_{DP}^{b}10^{cZ_{DR}} \tag{2}$$

2.4 MRMS Radar-Derived Rotation Tracks

The MRMS (NOAA National Severe Storms Laboratory) radar-derived rotation tracks were incorporated into the 1-hour mean Z_H plots to quantify the correlation between rotation tracks associated with the tropical supercells and enhanced Z_H. Rotation tracks were derived from the azimuthal shear field from the KHGX radar and is obtained by using a linear least squares derivative method (Smith et al. 2016) on the radial velocity from the radar site. The tracks have a temporal resolution of 2 minutes, with a spatial resolution of 555 x 504 m. Further, both 0-2 km and 3-6 km rotation tracks were analyzed to examine the low-level and mid-level rotation associated with these supercells. The rotation track data used the 60-minute data at the top of each hour to represent the swaths of enhanced azimuthal shear that occurred within the previous hour. The tracks were then superimposed atop 1-hour mean values of the 2 km polarimetric radar variables. Only values above 0.016 s^{-1} were displayed to to minimize noise and isolate supercellular features.

2.5 Additional Data

The Hurricane Database (HURDAT) Best Track data was used to plot the track and varying intensity of Harvey through its entire evolution (Fig.2). Each data point has a 6-hour temporal resolution, which represents the center of circulation of Harvey. Sea surface temperature magnitudes and anomalies were computed using the NOAA Optimum Interpolation Sea Surface Temperature V2 dataset with a 1^o x 1^o global grid (Reynolds et al. 2002). The anomalies were computed by subtracting the monthly mean from each day since SSTs generally vary over a larger time scale due to their high specific heat capacity (Fig.3).

Filtered storm reports from the Storm Prediction Center (SPC) were used to identify locations of tornado reports associated with the outer rainbands of Harvey from 26-28 August. Finally, observed radiosonde data from the CRP and LCH upper-air sites were plotted from 0000 UTC on 26 August throughout 1200 UTC on 28 August using MetPy plotting software (May et al. 2008 - 2017). These upper-air observations were used to calculate the WCD consistent with the methodology used by Vitale and Ryan 2013, which accounts for the presence of of supercooled liquid drops below the -10^o C level. Table 1 shows daily mean values of TPW, with the anomalies calculated from the Storm Prediction Center Sounding Climatology (NOAA/NWS SPC) using the 1989-2014 mean TPW at CRP, and the 1948-2014 climatology at LCH.

3 Results

3.1 Precipitation Efficiency

During the 6-day period in which Harvey was located over southeast Texas, TPW anomalies largely exceeded 1.5σ - 2.5σ (Fig.4). These values are also consistent with observed radiosonde data from CRP (Fig.5) and LCH (Fig.6), shown in Table 1. Here, moist adiabatic tropospheric profiles throughout the time period were observed with "skinny" convective available potential energy (CAPE) (e.g., Davis 2001; Jessup and DeGaetano 2008; Schroeder et al. 2016). This is indicative of slow ascent rates and a longer cloud droplet residence time compared to the "fat" CAPE profiles that are typically associated with mid-latitude, continental supercells (e.g., Vitale and Ryan 2013; Schroeder et al. 2016), translating to a more efficient drop growth process via collision-coalescence.

Additionally, a deeper warm cloud depth maximizes the vertical extent of warm rain processes, which further act to maximize PE at the surface (Hisham Mohd Anip and Market 2007). Table 2 shows how the WCD varied throughout the evolution of Harvey, with WCD values consistently in excess of 6000 m from 26-30 August. Further, it can be seen from Figure 7 that the areas of maximum PE were largely collocated with the central location of Harvey. While measures of efficiency typically range from 0-100%, this calculation of PE can exceed 100% due to the addition of horizontal moisture flux convergence and latent heat fluxes, which act to add mois-

ture to the vertical column through horizontal and vertical moisture advection and condensation. This is confirmed via Figure 8 which displays the significant latent heat fluxes over southeast Texas that acted to increase total column water vapor. Because the sign of the flux is dependent on direction, a negative latent heat flux corresponds to a downward moisture flux, which ultimately results in condensation and vast amounts of latent heat release. The regions of latent heat flux anomalies which exceeded -3σ relative to climatology were primarily located upstream of the areas of enhanced PE. The mean 10-m wind vectors are overlaid to provide a qualitative sense of the ongoing moisture advection over the region, acting to increase the amount of available water vapor in the vertical column. Additionally, Figure 9 illustrates the collocation of positive horizontal moisture flux convergence anomalies with the regions of enhanced PE.

Tables 1 and 2 demonstrate the relationship between PE, TPW anomalies, and WCD. The greatest TPW anomaly, PE, and WCD were temporally collocated at CRP on 26 August. Additionally, the greatest TPW anomaly at LCH was temporally offset from the times of highest PE and deepest WCD by one day. However, qualitatively there exists a positive relationship between positive TPW anomalies, WCDs greater than 6000 m, and PE greater than 100%. This demonstrates that anomalously high total column water vapor and deep warm cloud depths maximized the extent of warm rain processes and acted to enhance PE at the surface.

3.2 Polarimetric Radar Analysis

Figures 10 displays the 6-hour mean values of Z_H, Z_{DR}, and K_{DP} at 3 km over Houston from 27-28 August. The Z_H values ranged from 35-45 dBZ to the north of Houston and 20-30 dBZ to the south. A similar spatial pattern existed with Z_{DR}, with values exceeding 1 dB to the north of Houston, and values between 0-0.5 dB to the south. In addition, notable swaths of K_{DP} exceeding 1 deg/km occurred over the same regions experiencing the enhanced positive Z_H and Z_{DR}. The combination of these polarimetric radar variables imply a large number concentration of larger drops in a sample volume to the north of Houston. Although the larger values of Z_{DR} in the northern area of Houston implies the presence of larger drops and perhaps some contamination of melting precipitation, Z_{DR} of 1-1.5 dB is still characteristic of small drops and warm rain (e.g., Squires 1956; Ulbrich and Atlas 2008; Carr et al. 2017). In addition, this region was spatially collocated with the region of PE exceeding 100%. This overall pattern was also observed from 28-29 August across the region with slightly lower values of all three variables as compared to the 27th (figure not shown).

A time-height curtain of Z_H, Z_{DR}, and K_{DP} over Houston from 27-28 August to provides insight to the vertical extent of precipitation processes (Fig.11). These profiles can help identify dynamic features such as the melting layer height and columns of enhanced Z_{DR} and K_{DP} extending above the melting layer, implying robust convective updrafts. From 27-28 August, Z_H yielded values exceeding 45 dBZ for more than half the period. This was not surprising given Houston received nearly 500 mm

of rain on this day, with a maxima in PE exceeding 300% located over the city and extending to the north and west. Similarly, numerous Z_{DR} columns coexist with the regions of high Z_H and Z_{DR} with values as high as 1.5 dB. A similar pattern existed in the K_{DP} field, implying a large concentration of larger drops was being lofted above the melting layer. An upward displacement of the melting layer was also observed coincident with convection over the area which acted to increase the WCD and increase PE at the surface.

One interesting difference in the polarimetric radar fields exists over Liberty from 29-30 August (Fig.12). The Z_H field ranges from 20-40 dBZ and is characteristic of stratiform precipitation. From 0600-1200 UTC, Z_{DR} ranges from 0-1 dB, and K_{DP} ranges from 0-0.5 deg/km below the melting layer which is reflective of a larger number concentration of small drops, and is expected in an environment with a deep warm cloud depth. From 1800-0000 UTC, similar values of Z_H remained over the region, however Z_{DR} was much larger, with values between 1-2 dB, whereas K_{DP} was near 0 deg/km. This was consistent with a small number concentration of large drops, and more characteristic of mid-latitude, continental precipitation that involves additional cold rain processes.

These vertical profiles also infer information regarding whether drop growth was occurring versus drop breakup. An increase in Z_{DR} towards the ground would imply drop growth via collision-coalescence as an increase in drop size results in raindrops becoming increasingly oblate with a greater horizontal dimension when compared to

the vertical (e.g., Kumjian 2012; Carr et al. 2017). Similarly, an decrease in Z_{DR} and increase in Z_H towards the surface implies a collision-coalescence and drop breakup balance (e.g., Kumjian 2012; Carr et al. 2017) Figure 13 shows 6-hour means of the vertical profiles of Z_H, Z_{DR}, K_{DP}, and ρ_{hv} over Houston from 27-29 August. From 27-28 August, Z_{DR} decreased towards to surface except for the 0600-1200 UTC time frame, yet Z_H increased towards the ground. This decrease in Z_{DR} and increase in Z_H with decreasing height is reflective of a balance between collision-coalescence and drop breakup. However, from 28-29 August, Z_{DR} increased towards the surface at all times. This is characteristic of drop growth and collision coalescence, and is expected to occur in a tropical cyclone environment.

3.3 Rotation Track Analysis

The 1-hour mean values of Z_H at 2 km were also analyzed for the study domain and Figure 14 reveals swaths of enhanced Z_H of approximately 50-55 dBZ over Houston. The hourly MRMS 3-6 km rotation were overlaid for the same time period in order to determine whether supercells within the outer rainbands and the swaths of enhanced Z_H were present and producing excessive precipitation. From 0300-0400 UTC on 27 August, training supercells moving northward off the Gulf of Mexico were located over eastern portions of Houston and yielded swaths characterized by 1-hour mean values of Z_H near 50 dBZ, values of Z_{DR} between 1-1.5 dB, and K_{DP} values of 1.5-2 deg/km. This is consistent with a larger average drop size within a sample

volume in relation to the larger-scale mean Z_{DR} distribution, and is consistent with the spatial correlation between a large number concentration of larger drops within a radar volume being collocated with the highest values of PE. This is largely different than the lower PE associated with mid-latitude, continental convection. Additional training supercells occurred from 0600-0700 UTC on 28 August east of Liberty with Z_H values near 45 dBZ, Z_{DR} values near 1.5 dB, and maximum K_{DP} values of 1.5 deg/km. The overlaid azimuthal shear shows that the convective elements over these locations were also rotating, implying that supercells were responsible for producing these enhanced values of Z_H, Z_{DR}, and K_{DP}.

3.4 Quantitative Precipitation Estimation in Tropical Supercells

Figure 15 shows the 1-hour mean rainfall rates within these training supercells was as high as 85 mm per hour, with widespread rainfall rates exceeding 50 mm per hour within the line of supercells from 0300-0400 UTC on 27 August, extending 85 km inland from the coast. When averaged over the 0000-0600 UTC timeframe, the 6-hour mean rainfall rates were as high as 45 mm per hour to the southeast of Houston where the training supercells in the outer bands were occurring. This translates to 6-hour rainfall accumulations nearing 250 mm over the same area. Further, throughout the 24 hour period, this $R(K_{DP}, Z_{DR})$ relationship estimated rainfall accumulations as high as 425 mm, with widespread rainfall totals of 200-400 mm over the region

where training supercells did not occur.

4 Discussion

Landfalling tropical cyclones produce excessive rainfall which can lead to catastrophic flooding, especially if steering flow is weak and the remnant TC remains stationary for an extended period of time (Rappaport 2000). Even after TCs become less organized and lose their compact circulation as they move inland, the deadliest hazard is often freshwater flooding such as events including tropical storms Charley (1998), Alberto (1994), and Amelia (1978) (Rappaport 2000).

Excessive rainfall occurs where rain is heaviest for the longest period of time (Doswell et al. 1996). A synoptic-scale environment characterized by high TPW and large precipitation accumulation at the surface is said to have a high PE (Ye et al. 2014). Because the large-scale environment over southeast Texas from 25-31 August yielded TPW anomalies exceeding $1.5\sigma - 2.5\sigma$, Harvey remained quasi-stationary in a region conducive for enhanced PE. As such, observed rainfall totals were greater than 1000 mm over a region spanning nearly 40,000 km^2.

Given the extended duration of the event and the proximity of Harvey to the KHGX WSR-88D, polarimetric radar observations of Z_H, Z_{DR}, and K_{DP}, were used to quantify precipitation processes in the outer rainbands. The polarimetric radar observations were able to capture the evolution and extent of the warm rain processes that contributed to the excessive rainfall event over southeast Texas. Widespread

Values of Z_H greater than 30 dBZ existed over the Houston area from 27-29 of August. However, Z_H alone does not reveal much about the hydrometeor size, shape, and orientation (e.g., Seliga and Bringi 1976; Herzegh and Jameson 1992; Ryzhkov et al. 2005a; Ryzhkov et al. 2005b; Kumjian 2013a), which can provide information about the ongoing precipitation processes (Didlake and Kumjian 2017). However when combining the Z_H field with the observed 6-hour mean Z_{DR} values near 0.5 dB and 6-hour mean K_{DP} values of 0.5 degrees/km, it can be inferred that a relatively large concentration of small drops contributed to the excessive precipitation event over southeast Texas. The synoptic-scale environment and resultant aforementioned Z_H, Z_{DR}, and K_{DP} values that resulted in high PE was conducive to an excessive precipitation event that produced widespread rainfall totals 100-200 mm over southeast Texas from 27-28 August.

While widespread rainfall rates of 10-20 mm per hour occurred due to the anomalously moist conditions on the synoptic scale, the heaviest rainfall rates and precipitation totals occurred within training supercells in the outer rainbands of Harvey. Polarimetric radar observations can also provide useful information regarding enhanced rainfall rates in convective storms through identification of Z_{DR} and K_{DP} columns (Homeyer and Kumjian 2015). These columns of enhanced Z_{DR} and K_{DP} can help identify large supercooled drops being lofted by convective updrafts (e.g., Herzegh and Jameson 1992; Loney et al. 2002; Kumjian et al. 2014), and can help distinguish embedded convective features from stratiform elements within the outer

rainbands (e.g., Griffin et al. 2014; Didlake Jr. and Kumjian 2018)

The supercells in Harvey were identified using 3-6 MRMS rotation tracks and were collocated with swaths of enhanced polarimetric radar variables. Within these supercells from 0300-0400 UTC on 27 August, the 1-hour mean values of Z_H, Z_{DR}, and K_{DP} were as high as 50 dBZ, 1.25 dB, and 2 degrees/km. These results are consistent with those in Nielsen and Schumacher 2018, where mesocyclones were found to be responsible for enhanced rainfall rates at the surface. Figure 16 shows the training nature of the supercells which acted to increase the temporal component of flooding via the locally enhanced PE and rainfall rates. The $R(K_{DP}, Z_{DR})$ relationship highlights a swath of 1-hour mean rainfall rates as high as 85 mm per hour associated with the training supercells. When examining the 6-hour mean rainfall rate, the localized swath of 40-45 mm per hour rainfall rates southeast of Houston can be identified within the widespread area of 10-20 mm per hour rainfall rates which can be attributed to the large-scale environment that was favorable for excessive rainfall coincident with the training supercells. Additionally, numerous instances of supercell mergers occurred within the outer rainbands from 02-04 UTC on 27 August, which acts to merge two different drop size distributions and increase precipitation efficiency (e.g., Marwitz 1972; Markowski and Richardson 2010).

However, supercells within the outer rainbands of Harvey were determined to be responsible for two localized swaths of rainfall accumulations of 300-400 mm. This is consistent with Nielsen and Schumacher 2018 who demonstrated that extreme rainfall

accumulations are often closely collocated with mesovortices in mid-latitude supercell thunderstorms. One reason that supercells are often responsible for excessive precipitation is that they contain a sustained source for ascent via non-linear dynamic perturbation pressure gradient forces (e.g., Weisman and Klemp 1984; Doswell et al. 1996). W. Newton 1966 hypothesized that PE is enhanced in deep, saturated vertical columns, limiting dry air entrainment and therefore evaporation. Given this convection contained sustained, rotating updrafts in an area of enhanced PE, the resultant training supercells contributed most to the catastrophic rainfall that occurred over Houston.

4.1 Impacts

It is not surprising that the torrential rainfall rates of up to 85 mm per hour in these training supercells produced catastrophic urban and river flooding particularly to the southeast of Houston. Given this region is located 0-10 meters above sea level and the 100 mm of rainfall that this region saw on the previous day, this region may be even more prone to flooding compared to areas further north such as Downtown Houston.

While the hydrometeorological impacts of these embedded rotating features were by far the greatest hazard associated with Harvey (Edwards et al. 2018), multiple tornadoes were reported primarily to the south and west of Houston from 26-28 of August (Fig. 16). This is not surprising since the Houston area remained in the right-front quadrant of Harvey for an extended period of time, which McCaul 1991 deemed

the most favorable tornado environment in TCs when considering low-level shear and helicity, and is highly correlated with tornado frequency. Additionally, there are typically higher values of CAPE in the outer rainband portions of TCs which allows for a greater potential for stretching of low-level storm relative helicity (Edwards 2012). The constraint of TC tornadoes being limited to the outer rainbands is due to cloud cover being more prominent closer to the TC center, which limits diabatic heating via insolation and therefore buoyancy. Lastly, Edwards 2012 determined that operational evidence and experience shows that TC supercells commonly develop offshore and then move inland, with tornadogenesis occurring over water or during landfall. Due to Harvey's location over the Gulf of Mexico just south of the Houston area, this allowed for an extended period in which supercells moved onshore and impacted highly populated areas. As a result, Harvey resulted in Houston being in a tornado watch for 60 hours and is the longest period of time in which a mesoscale area has remained in a continuous tornado risk (Edwards et al. 2018).

Not only is this dangerous due to the stronger wind speeds and airborne debris caused by tornadoes, but these features were tracking over low-lying flooded areas. This is concerning given that people might not have been able to have taken shelter in a basement or interior room given the vast amount of flooding that occurred in this region, leaving few options for a safe place to seek shelter (Edwards et al. 2018). Additionally, Edwards 2012 found that the effects of TC tornadoes can often be masked by storm surge along coastal areas and inland freshwater flooding. Another issue

arises operationally because TC supercells tend to have weaker rotational features compared to mid-latitude supercells, and are more difficult to identify on radar and tend to be short-lived (Edwards 2012).

4.2 Limitations

Coarsely-spaced radiosonde observations and reanalysis data that are used to quantify TPW introduces some limitations when relating PE to a high temporal resolution dataset such as the NEXRAD WSR-88D polarimetric radar observations. Because PE is dependent on TPW, it would be useful to obtain hourly measurements of TPW to perform hourly spatial distributions of PE. This would allow for a more precise spatial correlation of PE and means of polarimetric radar variables.

One potential issue arises when compositing polarimetric radar variables close to the surface as ground clutter can often bias these observations and obscure the meteorological signals. This can be problematic since PE is calculated using accumulated precipitation observations at the surface, whereas the radar observations are analyzed at 2-3 km above ground level to avoid contamination from non-meteorological scatterers. Future analyses could remove these artifacts by setting a threshold greater than 0.8 for ρ_{hv}, as precipitation in tropical cyclones tends to be uniform in size, yielding ρ_{hv} near 1 in the absence of melting precipitation.

A limitation to the QPE method is that it does not perform well in areas of light rain, which did occur in between supercells and outer rainbands. Another constraint

is that the rainfall rate at 2 km may actually be an underestimation of the rainfall rate at the surface. This is because of additional drop growth towards the ground, which is due to collision-coalescence and results in an increase in Z_{DR} and K_{DP}.

5 Conclusion

Excessive precipitation occurred over Southeast Texas from Harvey and over 1000 mm of rain fell from 26-30 August, resulting in catastrophic urban and river flooding along with the loss of life and property. The heaviest precipitation totals typically collocate with regions that experience the heaviest precipitation for the longest period of time. Harvey remained nearly stationary over Houston and southeast Texas for 4 days, leading to a long duration excessive precipitation event. During that period, TPW anomalies exceeded 1.5σ - 2.5σ above the mean climatological value occurred throughout this period. Further, the PE $>$ 100% resulted from enhanced warm rain processes in addition to anomalously high horizontal moisture flux convergence, and negative latent heat flux anomalies (condensation), which increases the overall available moisture content in the vertical column.

When incorporating polarimetric radar observations from the KHGX WSR-88D platform, 6-hour temporal means of Z_H, Z_{DR}, and K_{DP} at 3 km from 27-28 August show the highest values of all three variables located to the north and west of Houston, with a mean Z_H of 35-45 dBZ, a mean Z_{DR} of 1-1.5 dB, and a mean K_{DP} near 1 deg/km. This is largely collocated with the highest values of PE during the same

time period, and is reflective of a relatively large number concentration of larger drops. While the drop size is larger in this region compared to areas to the south and east of Houston, this is still characteristic of small drops, which is expected in a tropical cyclone environment.

Time-height cross sections of these polarimetric variables over Houston also show columns of enhanced Z_H, Z_{DR}, and K_{DP} extending above the melting layer. This translates to convective updrafts lofting oblate hydrometeors above the melting level, which results in a greater PE at the surface. Finally, 6-hour mean vertical profiles of these profiles in addition to ρ_{hv} over Houston show Z_{DR} increasingly towards the surface below the melting layer. This is indicative of drop growth via collision-coalescence.

Additionally, swaths of 3-6 km rotation tracks were largely collocated with swaths of enhanced positive Z_H, Z_{DR}, and K_{DP}, implying that these supercells produced a large number concentration of large drops compared to the surrounding environment. The high PE in these supercells are contrary to the low PE that is typically found in mid-latitude, continental supercells. These supercells were also found to produce 1-hour mean rainfall rates of up to 85 mm/hour, and are likely one of the main drivers of the excessive precipitation event that occurred over the region. While this study incorporates polarimetric radar observations to quantify PE in Harvey, future work should use a similar framework in other landfalling tropical cyclones such as Irma, Florence, and Michael.

References

Anip, M. H. M., 2005: Dominant factors influencing precipitation efficiency in a continental mid-latitude location.

Ashley, S. T., and W. S. Ashley, 2008: Flood fatalities in the united states. *Journal of Applied Meteorology and Climatology*, **47 (3)**, 805–818, doi:10.1175/2007JAMC1611.1.

Austin, P. M., 1987: Relation between measured radar reflectivity and surface rainfall. *Monthly Weather Review*, **115 (5)**, 1053–1070, doi:10.1175/1520-0493(1987)115⟨1053:RBMRRA⟩2.0.CO;2.

Bowman, K. P., and C. R. Homeyer, 2017: Gridrad - three-dimensional gridded nexrad wsr-88d radar data. Research Data Archive at the National Center for Atmospheric Research, Computational and Information Systems Laboratory, Boulder CO.

Bringi, V. N., V. Chandrasekar, N. Balakrishnan, and D. S. Zrnić, 1990: An examination of propagation effects in rainfall on radar measurements at microwave frequencies. *Journal of Atmospheric and Oceanic Technology*, **7 (6)**, 829–840, doi:10.1175/1520-0426(1990)007⟨0829:AEOPEI⟩2.0.CO;2.

Brown, B. R., M. M. Bell, and A. J. Frambach, 2016: Validation of simulated hurri-

cane drop size distributions using polarimetric radar. *Geophysical Research Letters*, **43 (2)**, 910–917, doi:10.1002/2015GL067278.

Browning, K., 1977: The structure and mechanisms of hailstorms. *Meteorol. Monogr.*, **16**, 1–43, doi:10.1007/978-1-935704-30-0_1.

Carr, N., P. E. Kirstetter, J. J. Gourley, and Y. Hong, 2017: Polarimetric signatures of midlatitude warm-rain precipitation events. *Journal of Applied Meteorology and Climatology*, **56 (3)**, 697–711, doi:10.1175/JAMC-D-16-0164.1.

Center, N. N. W. S. N. R. O., 1991: Noaa next generation radar (nexrad) level 2 base data. NOAA National Centers for Environmental Information, doi:doi:10.7289/V5W9574V.

Chappell, R. P. S., Charles F., 1986: *Quasi-stationary convective events. Mesoscale Meteorology and Forecasting*, 289–290. American Meteorological Society, Boston MA, doi:https://doi.org/10.1007/978-1-935704-20-1_13.

Cifelli, R., V. Chandrasekar, S. Lim, P. C. Kennedy, Y. Wang, and S. A. Rutledge, 2011: A new dual-polarization radar rainfall algorithm: Application in colorado precipitation events. *Journal of Atmospheric and Oceanic Technology*, **28 (3)**, 352–364, doi:10.1175/2010JTECHA1488.1.

Crosson, W. L., C. E. Duchon, R. Raghavan, and S. J. Goodman, 1996: Assessment of rainfall estimates using a standard z-r relationship and the probability

matching method applied to composite radar data in central florida. *Journal of Applied Meteorology*, **35 (8)**, 1203–1219, doi:10.1175/1520-0450(1996)035⟨1203:AOREUA⟩2.0.CO;2.

Crum, T. D., and R. L. Alberty, 1993: The wsr-88d and the wsr-88d operational support facility. *Bulletin of the American Meteorological Society*, **74 (9)**, 1669–1688, doi:10.1175/1520-0477(1993)074⟨1669:TWATWO⟩2.0.CO;2.

Daly, C., R. P. Neilson, and D. L. Phillips, 1994: A statistical-topographic model for mapping climatological precipitation over mountainous terrain. *Journal of Applied Meteorology*, **33 (2)**, 140–158, doi:10.1175/1520-0450(1994)033⟨0140:ASTMFM⟩2.0.CO;2.

Davis, R. S., 2001: Flash flood forecast and detection methods. *Meteorological Monographs*, **50**, 481–526, doi:10.1175/0065-9401-28.50.481.

Didlake, A. C., and M. R. Kumjian, 2017: Examining polarimetric radar observations of bulk microphysical structures and their relation to vortex kinematics in hurricane arthur (2014). *Monthly Weather Review*, **145 (11)**, 4521–4541, doi:10.1175/MWR-D-17-0035.1.

Didlake Jr., A. C., and M. R. Kumjian, 2018: Examining storm asymmetries in hurricane irma (2017) using polarimetric radar observations. *Geophysical Research Letters*, **45 (24)**, 13,513–13,522, doi:10.1029/2018GL080739.

Doswell, C. A., H. E. Brooks, and R. A. Maddox, 1996: Flash flood forecasting: An ingredients-based methodology. *Weather and Forecasting*, **11 (4)**, 560–581, doi: 10.1175/1520-0434(1996)011⟨0560:FFFAIB⟩2.0.CO;2.

Duda, J. D., and W. A. Gallus, 2010: Spring and summer midwestern severe weather reports in supercells compared to other morphologies. *Weather and Forecasting*, **25 (1)**, 190–206, doi:10.1175/2009WAF2222338.1.

Edwards, R., 2012: Tropical cyclone tornadoes: A review of knowledge in research and prediction. *Electronic Journal of Severe Storms Meteorology*, **7**, 1–61.

Edwards, R., S. Overpeck, G. R. Woodall, and C. J. Nowotarski, 2018: Tornadoes in hurricane harvey: Documentation and environmental analysis. *Electronic Journal of Severe Storms Meteorology*, 1–20.

Foote, G. B., and J. C. Fankhauser, 1973: Airflow and moisture budget beneath a northeast colorado hailstorm. *Journal of Applied Meteorology*, **12 (8)**, 1330–1353, doi:10.1175/1520-0450(1973)012⟨1330:AAMBBA⟩2.0.CO;2.

Giangrande, S. E., and A. V. Ryzhkov, 2008: Estimation of rainfall based on the results of polarimetric echo classification. *Journal of Applied Meteorology and Climatology*, **47 (9)**, 2445–2462, doi:10.1175/2008JAMC1753.1.

Griffin, E. M., T. J. Schuur, D. R. MacGorman, M. R. Kumjian, and A. O. Fierro, 2014: An electrical and polarimetric analysis of the overland reintensification of

tropical storm erin (2007). *Monthly Weather Review*, **142 (6)**, 2321–2344, doi: 10.1175/MWR-D-13-00360.1.

Herzegh, P. H., and A. R. Jameson, 1992: Observing precipitation through dual-polarization radar measurements. *Bulletin of the American Meteorological Society*, **73 (9)**, 1365–1376, doi:10.1175/1520-0477(1992)073⟨1365:OPTDPR⟩2.0.CO;2.

Hisham Mohd Anip, M., and P. Market, 2007: Dominant factors influencing precipitation efficiency in a continental mid-latitude location. *Tellus A*, doi:10.3402/tellusa.v59i1.14853.

Hitchens, N., and H. Brooks, 2012: Preliminary investigation of the contribution of supercell thunderstorms to the climatology of heavy and extreme precipitation in the united states. *Atmospheric Research*, **123**, doi:10.1016/j.atmosres.2012.06.023.

Homeyer, C. R., and M. R. Kumjian, 2015: Microphysical characteristics of overshooting convection from polarimetric radar observations. *Journal of the Atmospheric Sciences*, **72 (2)**, 870–891, doi:10.1175/JAS-D-13-0388.1.

Houze, R. A., 1997: Stratiform precipitation in regions of convection: A meteorological paradox? *Bulletin of the American Meteorological Society*, **78 (10)**, 2179–2196, doi:10.1175/1520-0477(1997)078⟨2179:SPIROC⟩2.0.CO;2.

Jessup, S. M., and A. T. DeGaetano, 2008: A statistical comparison of the properties of flash flooding and nonflooding precipitation events in portions of new

york and pennsylvania. *Weather and Forecasting*, **23 (1)**, 114–130, doi:10.1175/2007WAF2006066.1.

Kumjian, M., 2012: The impact of precipitation physical processes on the polarimetric radar variables.

Kumjian, M., 2013a: Principles and applications of dual-polarization weather radar. part i: Description of the polarimetric radar variables. *Journal of Operational Meteorology*, **1**, 226–242, doi:10.15191/nwajom.2013.0119.

Kumjian, M., 2013b: Principles and applications of dual-polarization weather radar. part ii: Warm- and cold-season applications. *Journal of Operational Meteorology*, **1**, 243–264, doi:10.15191/nwajom.2013.0120.

Kumjian, M., 2013c: Principles and applications of dual-polarization weather radar. part iii: Artifacts. *Journal of Operational Meteorology*, **1**, 265–274, doi:10.15191/nwajom.2013.0121.

Kumjian, M. R., A. P. Khain, N. Benmoshe, E. Ilotoviz, A. V. Ryzhkov, and V. T. J. Phillips, 2014: The anatomy and physics of zdr columns: Investigating a polarimetric radar signature with a spectral bin microphysical model. *Journal of Applied Meteorology and Climatology*, **53 (7)**, 1820–1843, doi:10.1175/JAMC-D-13-0354.1.

Loney, M. L., D. S. Zrnić, J. M. Straka, and A. V. Ryzhkov, 2002: Enhanced polarimetric radar signatures above the melting level in a supercell storm. *Journal of*

Applied Meteorology, **41 (12)**, 1179–1194, doi:10.1175/1520-0450(2002)041⟨1179:EPRSAT⟩2.0.CO;2.

Markowski, P., and Y. Richardson, 2010: *Mesoscale Meteorology in Midlatitudes*. John Wiley and Sons, doi:10.1002/9780470682104.

Marwitz, J., 1972: Precipitation efficiency of thunderstorms on the high plains. *J. Rech. Atmos.*, **6**, 367–370.

May, R., S. Arms, P. Marsh, E. Bruning, and J. Leeman, 2008 - 2017: Metpy: A Python package for meteorological data. Boulder, Colorado, doi:10.5065/D6WW7G29.

McCaul, E. W., 1991: Buoyancy and shear characteristics of hurricane-tornado environments. *Monthly Weather Review*, **119 (8)**, 1954–1978, doi:10.1175/1520-0493(1991)119⟨1954:BASCOH⟩2.0.CO;2.

Medlin, J. M., S. K. Kimball, and K. G. Blackwell, 2007: Radar and rain gauge analysis of the extreme rainfall during hurricane danny's (1997) landfall. *Monthly Weather Review*, **135 (5)**, 1869–1888, doi:10.1175/MWR3368.1.

Mesinger, F., and Coauthors, 2006: North american regional reanalysis. *Bulletin of the American Meteorological Society*, **87 (3)**, 343–360, doi:10.1175/BAMS-87-3-343.

Nielsen, E. R., and R. S. Schumacher, 2018: Dynamical insights into extreme short-

term precipitation associated with supercells and mesovortices. *Journal of the Atmospheric Sciences*, **75 (9)**, 2983–3009, doi:10.1175/JAS-D-17-0385.1.

Rappaport, E. N., 2000: Loss of life in the united states associated with recent atlantic tropical cyclones. *Bulletin of the American Meteorological Society*, **81 (9)**, 2065–2074, doi:10.1175/1520-0477(2000)081⟨2065:LOLITU⟩2.3.CO;2.

Rappaport, E. N., 2014: Fatalities in the united states from atlantic tropical cyclones: New data and interpretation. *Bulletin of the American Meteorological Society*, **95 (3)**, 341–346, doi:10.1175/BAMS-D-12-00074.1.

Rappaport, E. N., and J. J. Fernandez-Partagas, 1997: *History of the Deadliest Atlantic Tropical Cyclones Since the Discovery of the New World*, 93–108. Springer Berlin Heidelberg, Berlin, Heidelberg, doi:10.1007/978-3-642-60672-4_5.

Reynolds, R. W., N. A. Rayner, T. M. Smith, D. C. Stokes, and W. Wang, 2002: An improved in situ and satellite sst analysis for climate. *Journal of Climate*, **15 (13)**, 1609–1625, doi:10.1175/1520-0442(2002)015⟨1609:AIISAS⟩2.0.CO;2.

Rosenfeld, D., D. B. Wolff, and D. Atlas, 1993: General probability-matched relations between radar reflectivity and rain rate. *Journal of Applied Meteorology*, **32 (1)**, 50–72, doi:10.1175/1520-0450(1993)032⟨0050:GPMRBR⟩2.0.CO;2.

Ryzhkov, A., P. Zhang, H. Reeves, M. Kumjian, T. Tschallener, S. Trömel, and C. Simmer, 2016: Quasi-vertical profiles—a new way to look at polarimetric radar

data. *Journal of Atmospheric and Oceanic Technology*, **33 (3)**, 551–562, doi:10.1175/JTECH-D-15-0020.1.

Ryzhkov, A. V., 2007: The impact of beam broadening on the quality of radar polarimetric data. *Journal of Atmospheric and Oceanic Technology*, **24 (5)**, 729–744, doi:10.1175/JTECH2003.1.

Ryzhkov, A. V., S. E. Giangrande, and T. J. Schuur, 2005a: Rainfall estimation with a polarimetric prototype of wsr-88d. *Journal of Applied Meteorology*, **44 (4)**, 502–515, doi:10.1175/JAM2213.1.

Ryzhkov, A. V., T. J. Schuur, D. W. Burgess, P. L. Heinselman, S. E. Giangrande, and D. S. Zrnic, 2005b: The joint polarization experiment: Polarimetric rainfall measurements and hydrometeor classification. *Bulletin of the American Meteorological Society*, **86 (6)**, 809–824, doi:10.1175/BAMS-86-6-809.

Schroeder, A., J. Basara, J. M. Shepherd, and S. Nelson, 2016: Insights into atmospheric contributors to urban flash flooding across the united states using an analysis of rawinsonde data and associated calculated parameters. *Journal of Applied Meteorology and Climatology*, **55 (2)**, 313–323, doi:10.1175/JAMC-D-14-0232.1.

Seliga, T. A., and V. N. Bringi, 1976: Potential use of radar differential reflectivity measurements at orthogonal polarizations for measuring precipitation. *Journal of Applied Meteorology*, **15 (1)**, 69–76, doi:10.1175/1520-0450(1976)015⟨0069:PUORDR⟩2.0.CO;2.

Service, N. W., 2001: Tropical storm allison heavy rains and floods texas and louisiana june 2001.

Smith, J. A., M. L. Baeck, Y. Zhang, and C. A. Doswell, 2001: Extreme rainfall and flooding from supercell thunderstorms. *Journal of Hydrometeorology*, **2 (5)**, 469–489, doi:10.1175/1525-7541(2001)002⟨0469:ERAFFS⟩2.0.CO;2.

Smith, T. M., and Coauthors, 2016: Multi-radar multi-sensor (mrms) severe weather and aviation products: Initial operating capabilities. *Bulletin of the American Meteorological Society*, **97 (9)**, 1617–1630, doi:10.1175/BAMS-D-14-00173.1.

Squires, P., 1956: The micro-structure of cumuli in maritime and continental air. *Tellus A*, doi:10.3402/tellusa.v8i4.9040.

Testud, J., E. Le Bouar, E. Obligis, and M. Ali-Mehenni, 2000: The rain profiling algorithm applied to polarimetric weather radar. *Journal of Atmospheric and Oceanic Technology*, **17 (3)**, 332–356, doi:10.1175/1520-0426(2000)017⟨0332:TRPAAT⟩2.0.CO;2.

Ulbrich, C. W., and D. Atlas, 2008: Radar measurement of rainfall with and without polarimetry. *Journal of Applied Meteorology and Climatology*, **47 (7)**, 1929–1939, doi:10.1175/2007JAMC1804.1.

van Lier-Walqui, M., and Coauthors, 2016: On polarimetric radar signatures of deep convection for model evaluation: Columns of specific differential phase ob-

served during mc3e. *Monthly Weather Review*, **144 (2)**, 737–758, doi:10.1175/MWR-D-15-0100.1.

Vitale, J., and T. Ryan, 2013: Operational recognition of high precipitation efficiency and low-echo-centroid convection. *Journal of Operational Meteorology*, **1**, 128–143, doi:10.15191/nwajom.2013.0112.

W. Newton, C., 1966: Circulations in large sheared cumulonimbus. *Tellus A*, doi:10.3402/tellusa.v18i4.9690.

Weisman, M. L., and J. B. Klemp, 1984: The structure and classification of numerically simulated convective stormsin directionally varying wind shears. *Monthly Weather Review*, **112 (12)**, 2479–2498, doi:10.1175/1520-0493(1984)112⟨2479:TSACON⟩2.0.CO;2.

Ye, H., E. J. Fetzer, S. Wong, A. Behrangi, E. T. Olsen, J. Cohen, B. H. Lambrigtsen, and L. Chen, 2014: Impact of increased water vapor on precipitation efficiency over northern eurasia. *Geophysical Research Letters*, **41 (8)**, 2941–2947, doi:10.1002/2014GL059830.

Zhang, Y., L. Liu, H. Wen, C. Wu, and Y. Zhang, 2018: Evaluation of the polarimetric-radar quantitative precipitation estimates of an extremely heavy rainfall event and nine common rainfall events in guangzhou. *Atmosphere*, **9 (9)**, doi:10.3390/atmos9090330.

Zrnic, D. S., and A. V. Ryzhkov, 1999: Polarimetry for weather surveillance radars. *Bulletin of the American Meteorological Society*, **80 (3)**, 389–406, doi:10.1175/1520-0477(1999)080⟨0389:PFWSR⟩2.0.CO;2.

Zrnić, D. S., and A. Ryzhkov, 1996: Advantages of rain measurements using specific differential phase. *Journal of Atmospheric and Oceanic Technology*, **13 (2)**, 454–464, doi:10.1175/1520-0426(1996)013⟨0454:AORMUS⟩2.0.CO;2.

Appendix

Date	CRP TPW	CRP TPW Anomaly	LCH TPW	LCH TPW Anomaly
8/26	68.89	22.92	62.82	17.86
8/27	64.66	19.70	65.23	20.53
8/28	56.41	11.20	63.73	18.52
8/29	48.27	2.55	57.61	12.14

Table 1: TPW and TPW Anomalies (mm) from 26-30 August at Corpus Christi (CRP) and Lake Charles (LCH)

Date	CRP WCD	CRP PE	LCH WCD	LCH PE
8/26	6950	114.7	6350	17.9
8/27	6248	3.6	6428	98.7
8/28	6460	5.6	5940	267.5
8/29	6144	1.0	6401	56.4

Table 2: WCD (m) and PE (%) from 26-30 August at Corpus Christi (CRP) and Lake Charles (LCH)

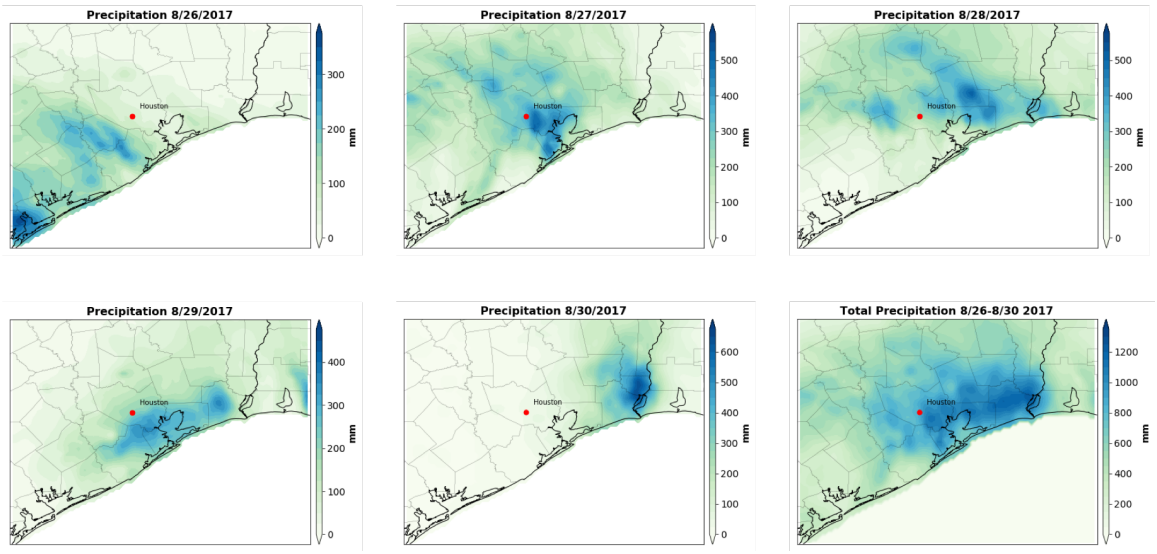

Figure 1: Accumulated daily precipitation from 26-30 August, and total accumulated precipitation from 26-30 Aug

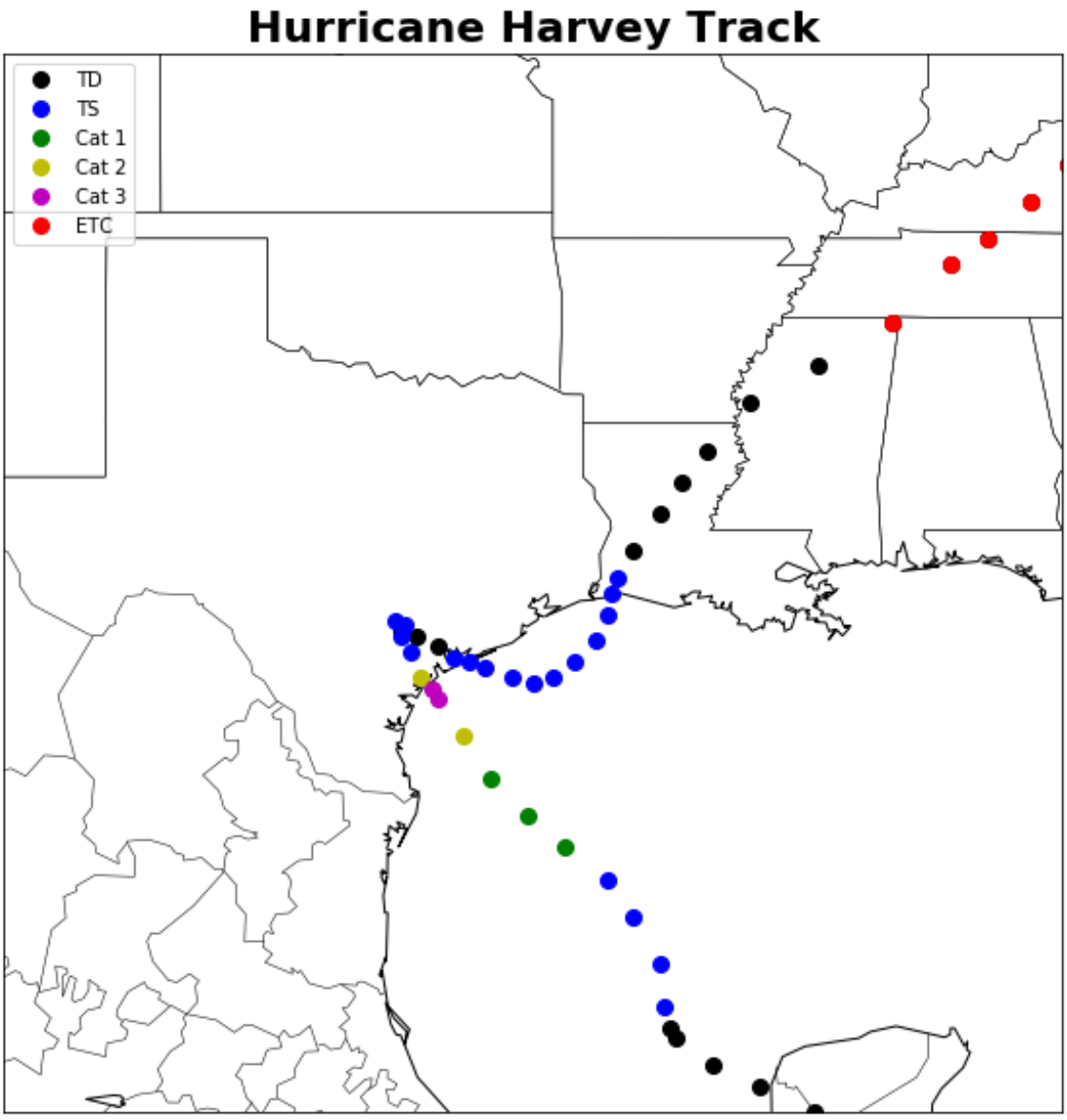

Figure 2: Hurricane Database (HURDAT) Best Track showing the track and categorical evolution of Harvey. Each point represents the center of circulation of Harvey. Points are spaced in 6-hour time increments.

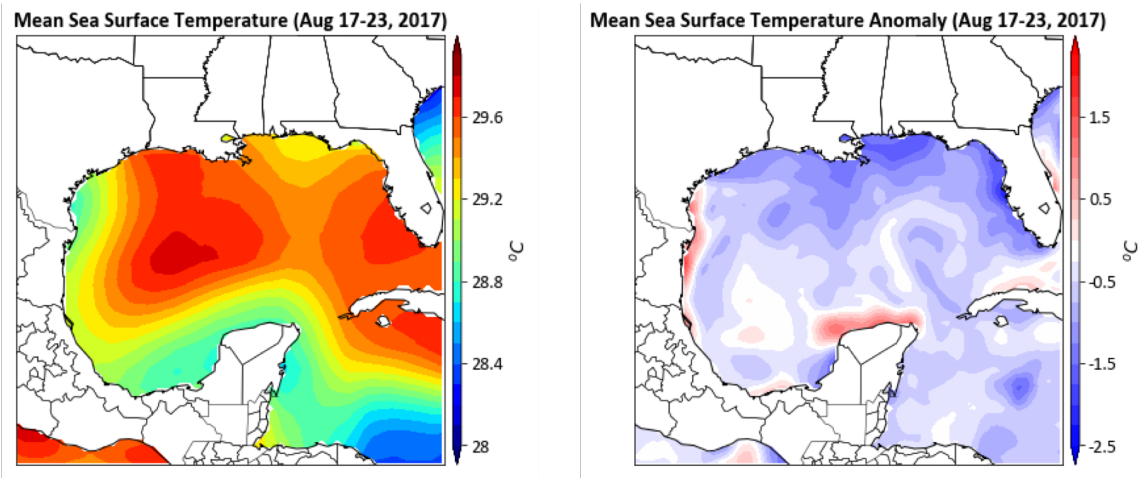

Figure 3: Mean Sea Surface Temperature (SST) from 17-23 August, and mean SST anomaly from 17-23 August, for the week prior to Harvey making landfall

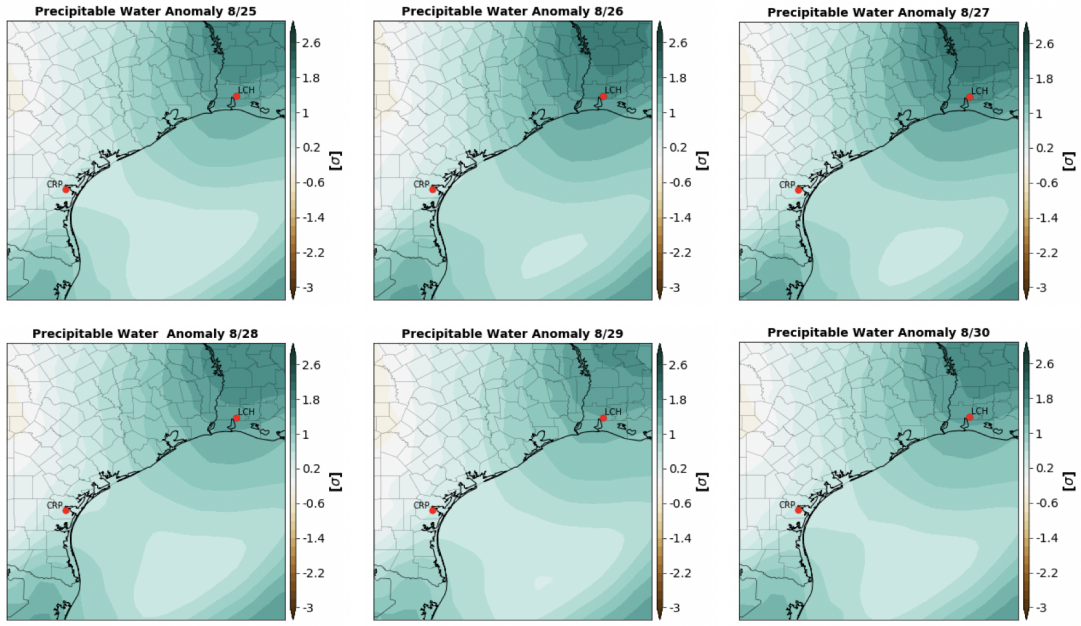

Figure 4: Total Precipitable Water (TPW) anomaly from 25-30 August standardized from 1979-2017 climatology

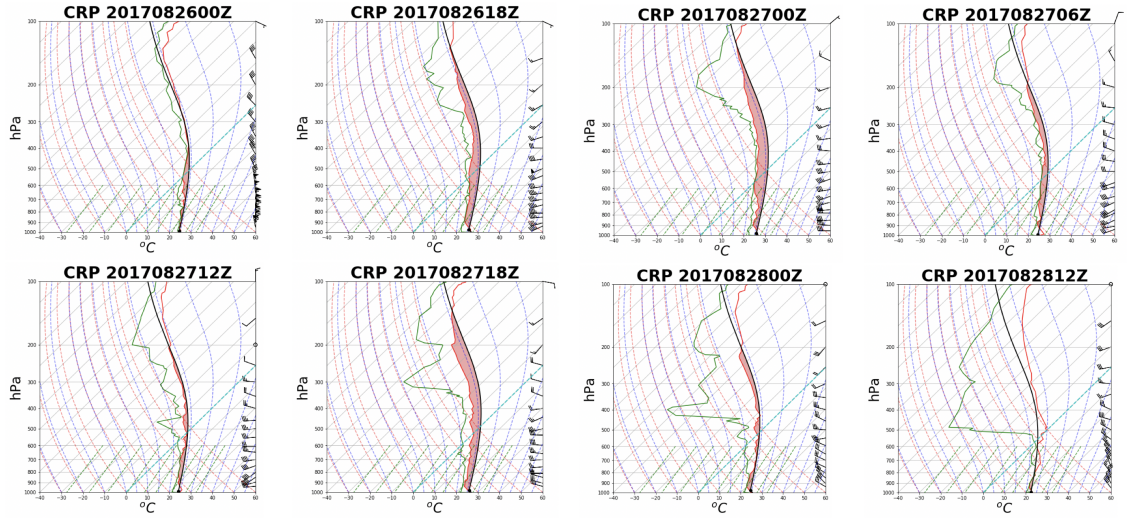

Figure 5: Observed soundings taken over Corpus Christi, Texas (CRP) from 00 UTC August 26 - 12 UTC August 28

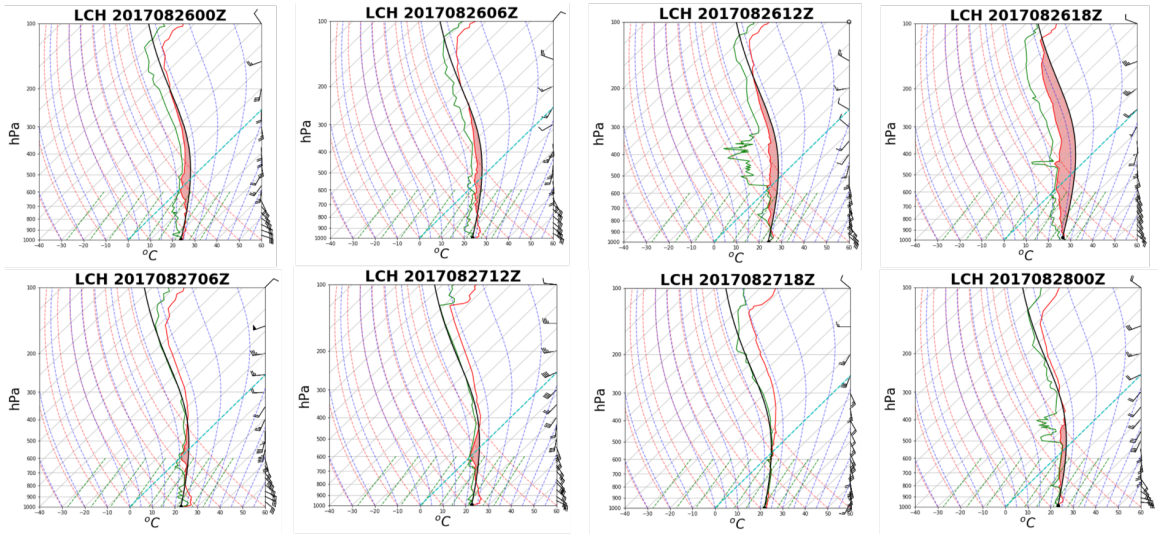

Figure 6: Observed soundings taken over Lake Charles, Louisiana (LCH) from 26-28 August

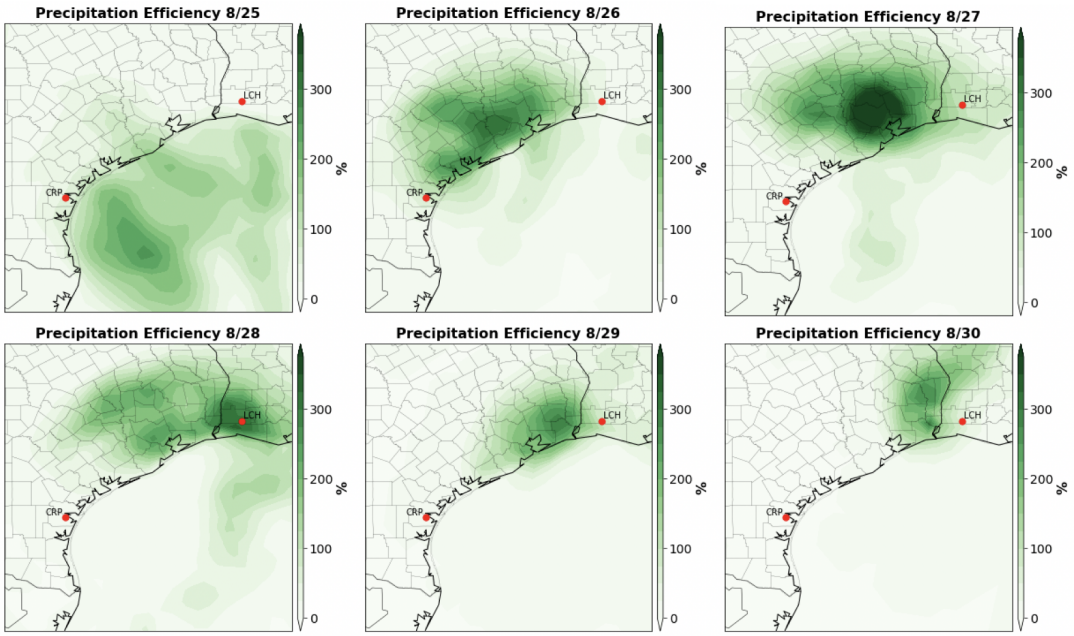

Figure 7: Precipitation Efficiency (PE) calculated using (1) from 25-30 August

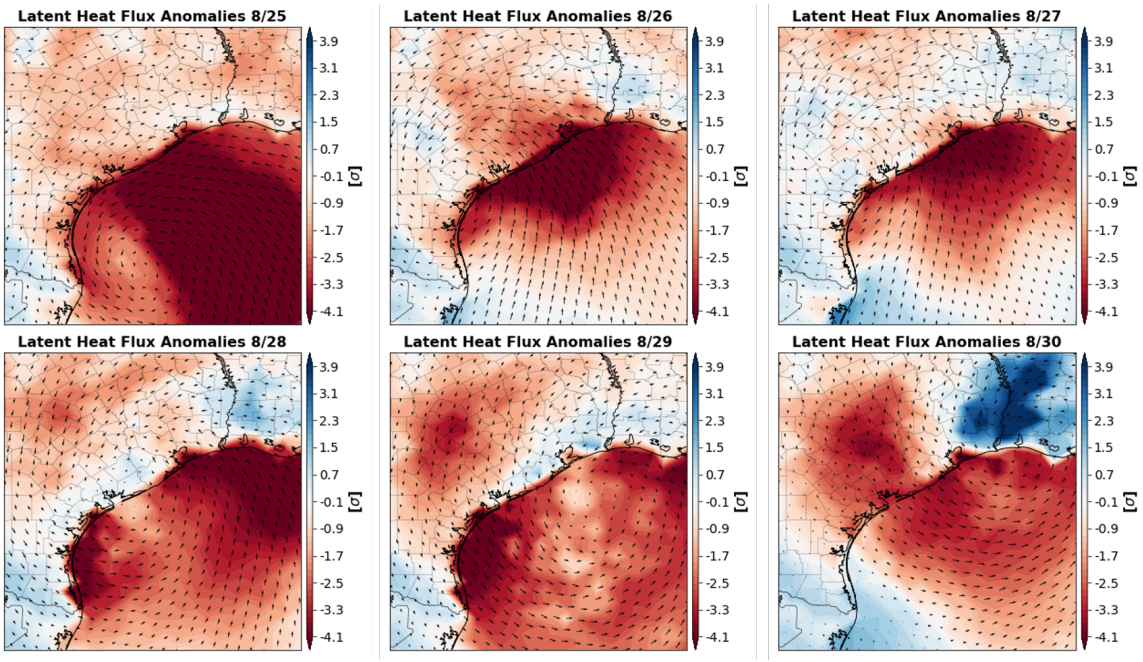

Figure 8: Latent heat flux anomalies from 25-30 August standardized from 1979-2017 climatology, with daily mean 10-m wind vectors

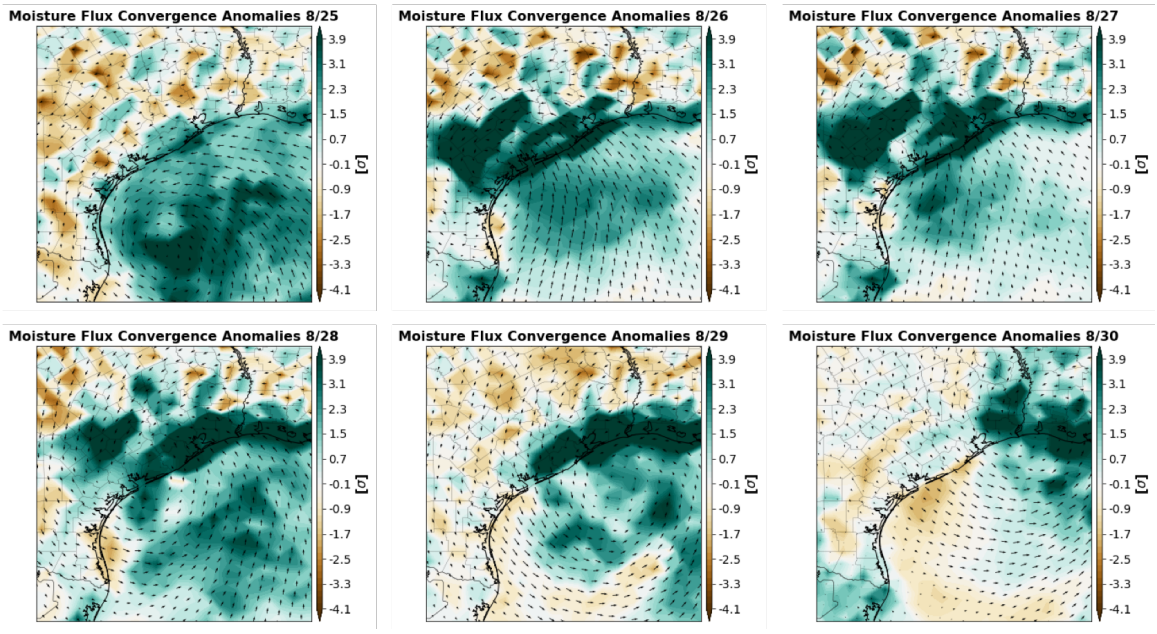

Figure 9: Moisture Flux Convergence anomalies from 25-30 August standardized from 1979-2017 climatology, with daily mean 10-m wind vectors

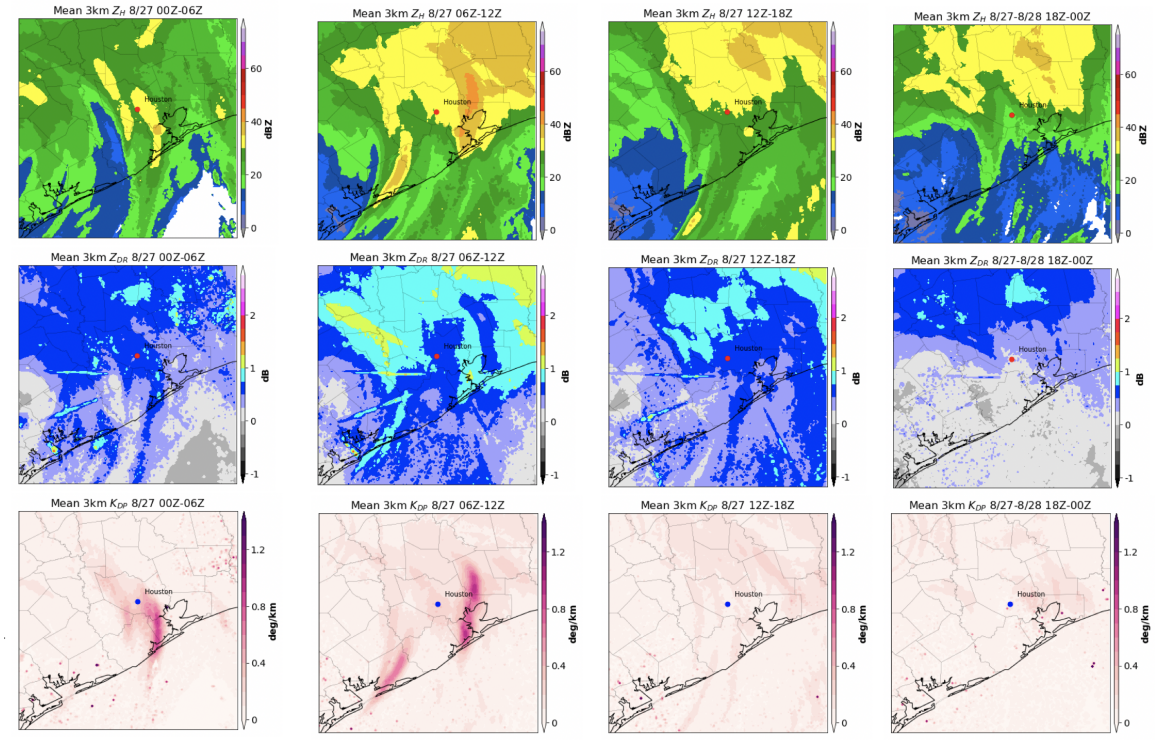

Figure 10: 6-hour means of 3 km Z_H, Z_{DR}, and K_{DP} from 26-27 August

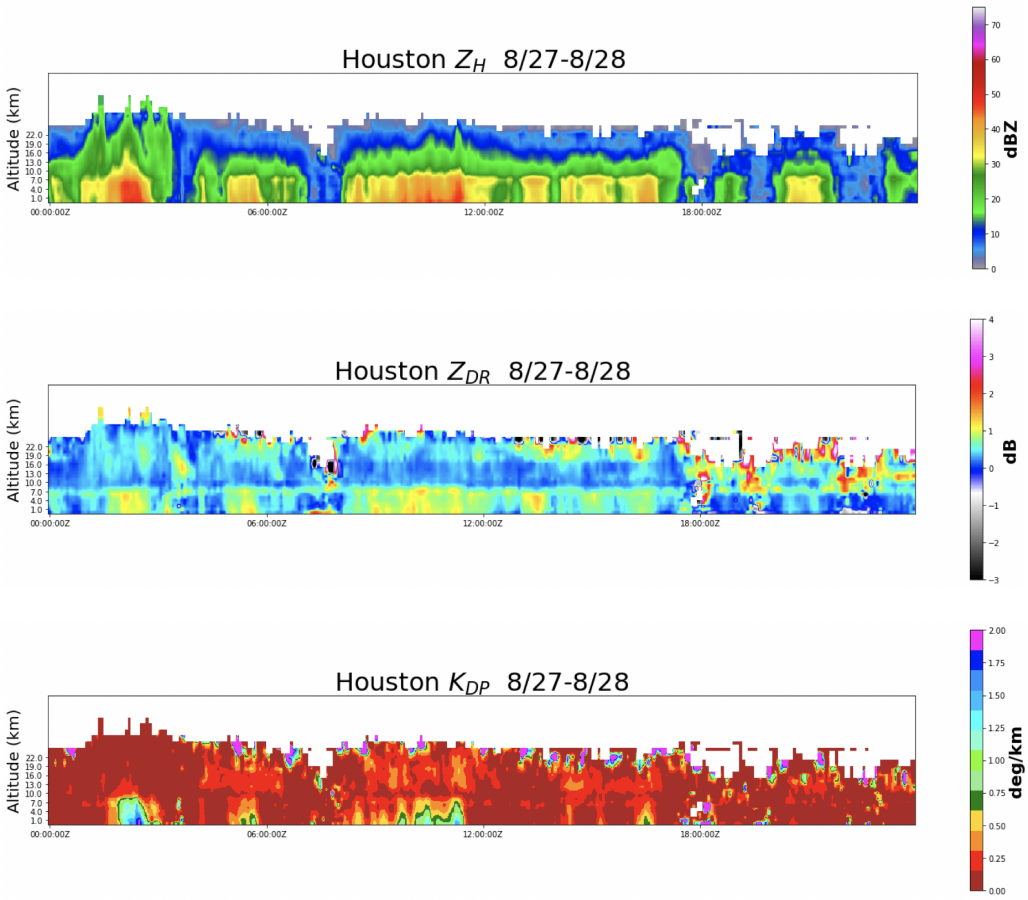

Figure 11: Time-height cross-sections of Z_H, Z_{DR}, and K_{DP} over Houston, Texas from 27-28 August

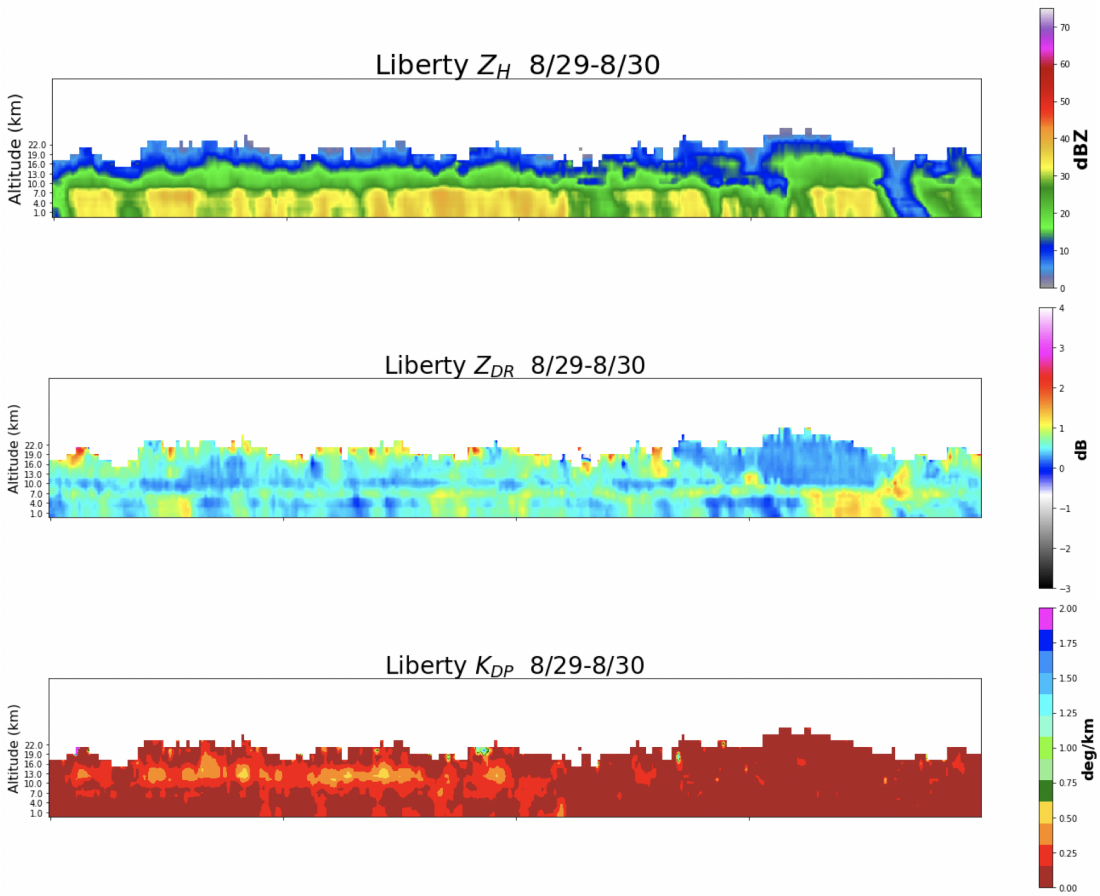

Figure 12: Time-height cross-sections of Z_H, Z_{DR}, and K_{DP} over Liberty, Texas from 29-30 August

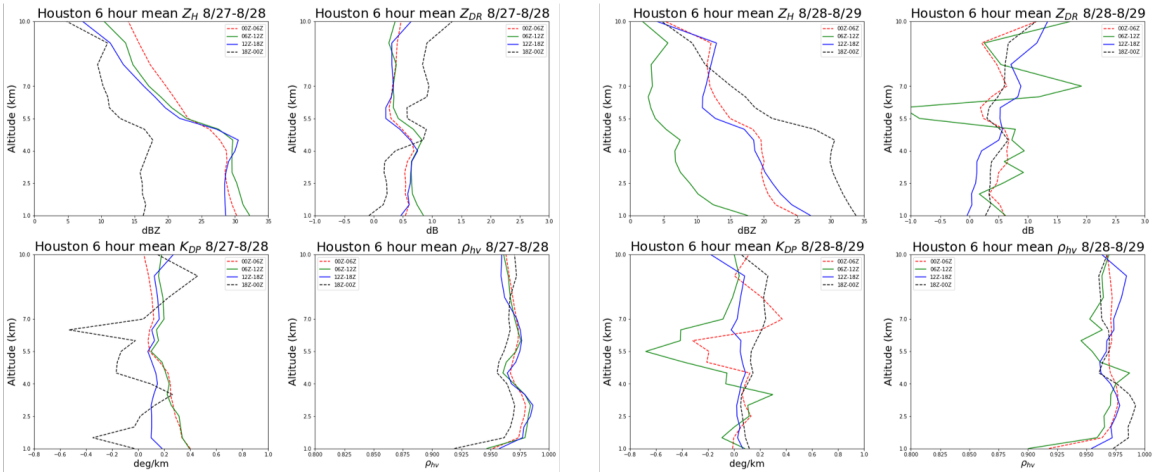

Figure 13: 6-hour mean vertical profiles of Z_H, Z_{DR}, K_{DP}, and ρ_{hv} over Houston from 27-28 August (left), and 28-29 August (right)

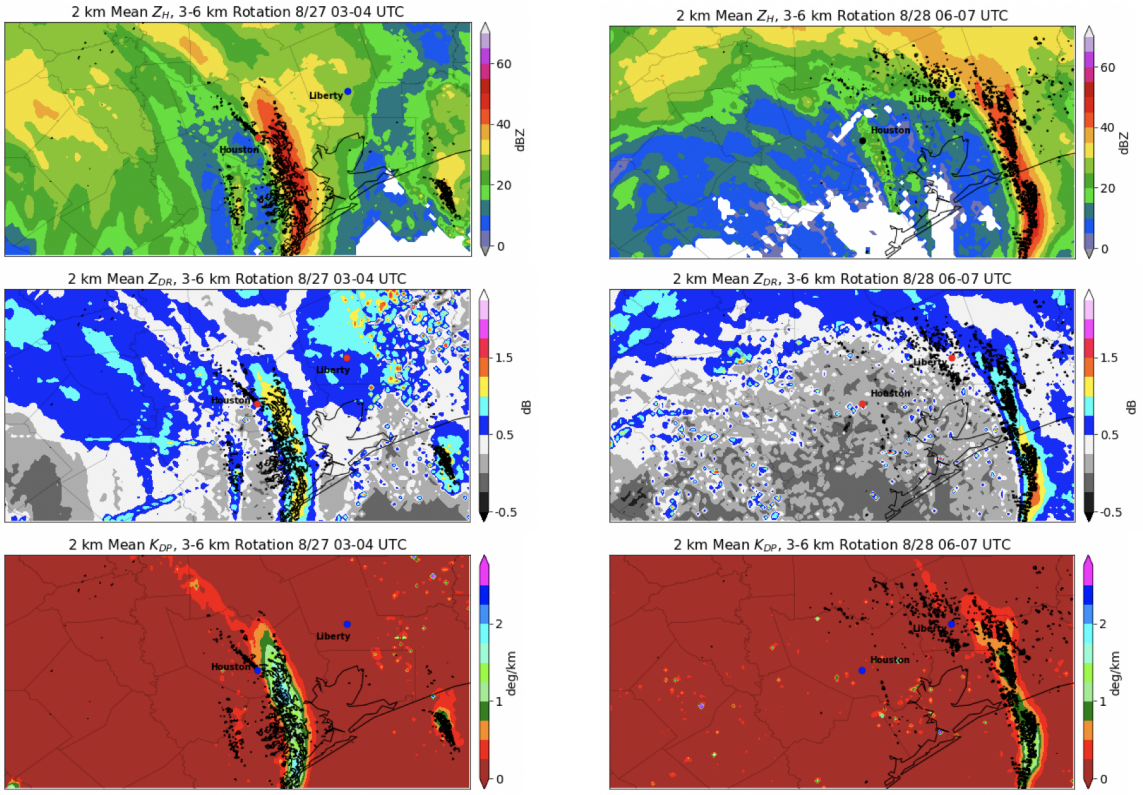

Figure 14: 1-hour means of 2 km Z_H, Z_{DR}, and K_{DP} from 03-04 UTC 27 August (left), and from 07-08 UTC 28 August (right), with 3-6 km hourly rotation tracks greater than $0.016s^{-1}$ (contours)

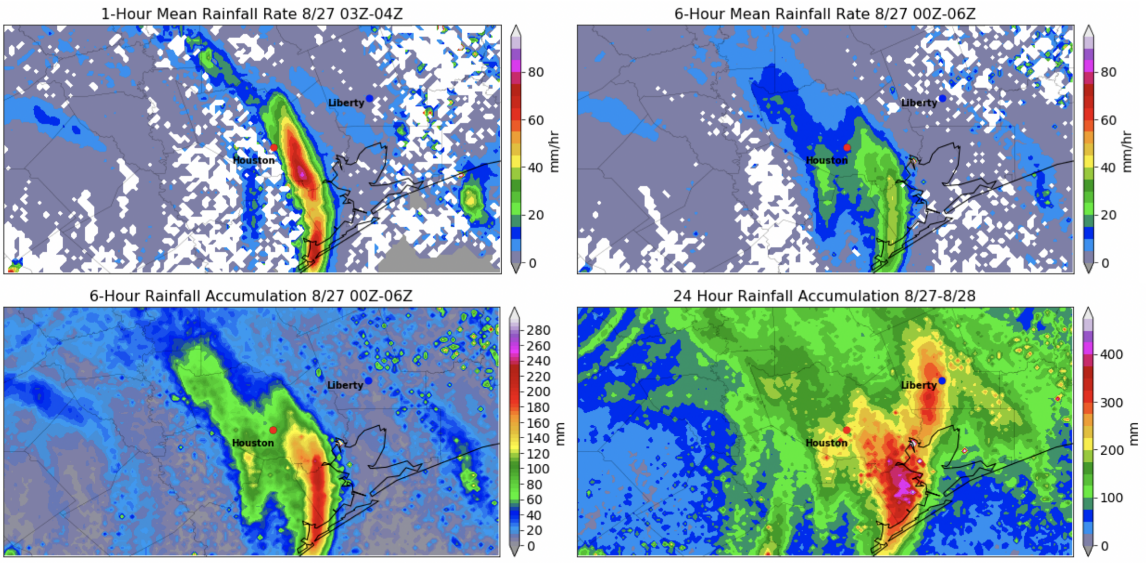

Figure 15: 1-hour and 6-hour mean rainfall rates from 03-04 UTC 27 August and 00-06 UTC 27 August using the aforementioned $R(K_{DP}, Z_{DR})$ relationship (top), and rainfall accumulation from 00-06 UTC 27 August and 27-28 August (bottom)

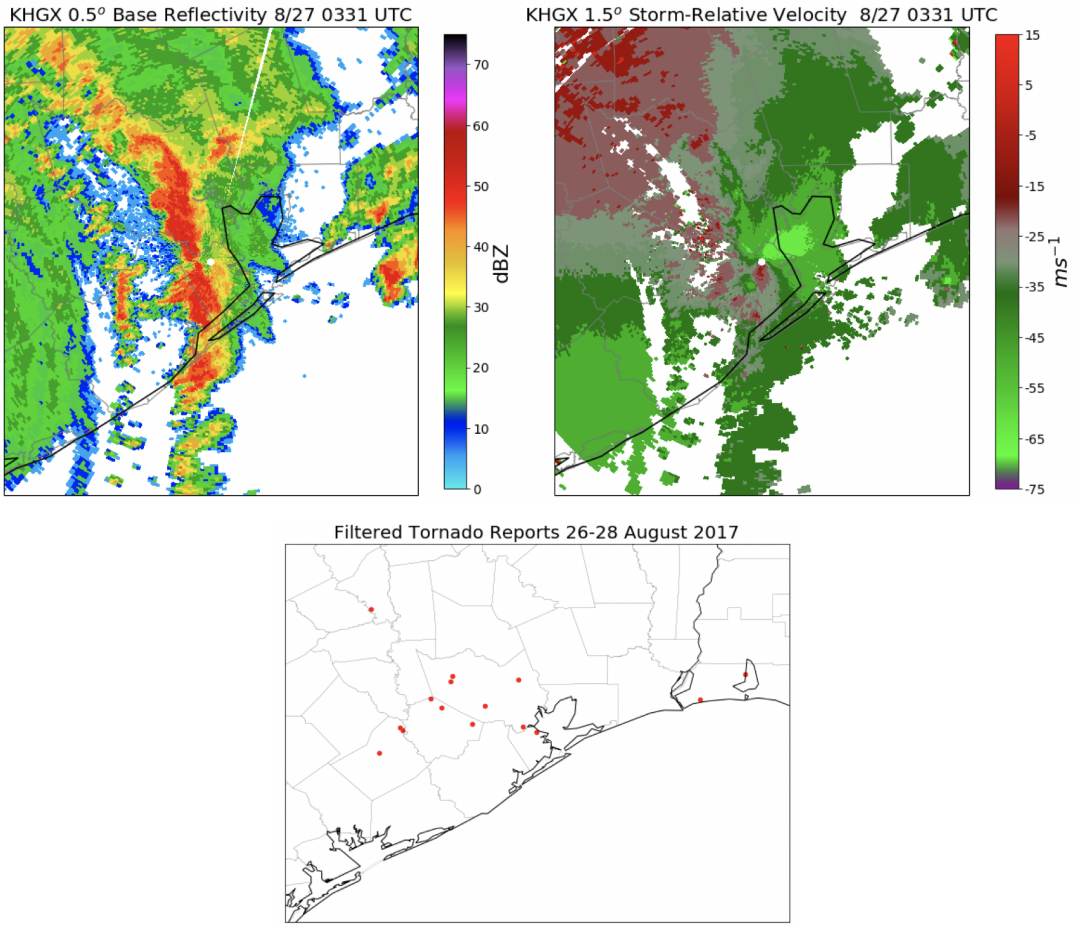

Figure 16: 0.5^o Z_H, 1.5^o storm-relative velocity from the KHGX WSR-88D at 0331 UTC 27 August showing the line of training supercells east of Houston, and SPC filtered tornado reports from 26-28 August